



# Düzce Üniversitesi Bilim ve Teknoloji Dergisi

*Araştırma Makalesi*

## Sliding Mode Control Based Supercapacitor Modeling for Dynamic Stability in DFIG Based Wind Turbines

 M. Kenan DÖŞOĞLU <sup>a,\*</sup>,  Uğur GÜVENÇ <sup>b</sup>,  Enes KAYMAZ <sup>c</sup>

<sup>a,b,c</sup> *Elektrik Elektronik Mühendisliği Bölümü, Mühendislik Fakültesi, Düzce Üniversitesi, Düzce, TÜRKİYE*

*\* Sorumlu yazarın e-posta adresi: kenandosoglu@duzce.edu.tr*

DOI: 10.29130/dubited.1020670

### ABSTRACT

The supercapacitor is among the elements commonly used to store energy as an important component in sustainable energy systems. In doubly fed induction generators (DFIGs), the supercapacitor is used to compensate voltage dips and damping oscillations. In this study, a different supercapacitor model was developed for system stability in a DFIG-based wind turbine connected to an infinite bus. In the development of the mathematical supercapacitor model, the lookup table was realized with the voltage-capacity relationship and sliding mode control. DFIG modeling with/without the developed supercapacitor was performed for symmetrical and asymmetrical fault situations, and the findings were then compared and interpreted in detail. The simulation study analysis was conducted in a MATLAB/SIMULINK environment. The developed supercapacitor model yielded impressive results in symmetrical and asymmetrical faults.

**Keywords:** *DFIG, supercapacitor modeling, lookup table, sliding mode control.*

## ÇBAG Tabanlı Rüzgar Türbinlerinde Dinamik Kararlılık için Kayan Kipli Kontrol Tabanlı Süperkapasitör Modellemesi

### Öz

Süperkapasitör, sürdürülebilir enerji sistemlerinde önemli bir bileşen olarak enerjiyi depolamak için yaygın olarak kullanılan elemanlar arasındadır. Çift beslemeli asenkron generatörlerde (ÇBAG), süperkapasitör, gerilim düşmelerini ve salınımların sönümlenmesini iyileştirmek için kullanılır. Bu çalışmada, sonsuz bir baraya bağlı olan ÇBAG tabanlı bir rüzgar türbininde sistem kararlılığı için farklı bir süperkapasitör modeli geliştirilmiştir. Matematiksel süperkapasitör modelinin geliştirilmesinde lookup table, gerilim-kapasite ilişkisi ve kayan kipli kontrol ile gerçekleştirilmiştir. Simetrik ve asimetric arıza durumları için, geliştirilen süperkapasitörlü ve süperkapasitörsüz DFIG modellemesi yapılmış ve elde edilen bulgular detaylı olarak karşılaştırılmış ve yorumlanmıştır. Benzetim çalışması analizi, MATLAB/SIMULINK ortamında gerçekleştirilmiştir. Geliştirilen süperkapasitör modeli simetrik ve asimetric arızalarda etkili sonuçlar vermiştir.

**Anahtar Kelimeler:** *ÇBAG, süperkapasitör modeli, lookup table, kayan kipli kontrol.*

# **I. INTRODUCTION**

The use of renewable energy technology has been increasing in recent years. Wind energy, in particular, has been in greater use than other renewable energy sources. High energy transfer capability technology is at the forefront in wind turbine applications. To achieve this capability at the maximum level, doubly fed induction generators (DFIGs) are used [1]. However, grid-connected DFIG-based wind turbines are very sensitive to certain transient stability situations and studies in the literature have developed various models to eliminate them. The Energy Storage Systems (ESS) model is one of the most widely used. Among the ESS elements is a supercapacitor that enables smooth output power and prevents oscillations. Constant power control is provided by using the supercapacitor model in DFIGs. Moreover, a management control unit has been developed to provide power tracking [2-5]. Supercapacitors are used in DFIGs to obtain constant output power as well as to prevent frequency changes of switching elements in the converter circuit. When monitoring the maximum power point with the supercapacitor, the responses to the change in wind speed, tower shadow, and the protection units were examined [6-7]. The supercapacitor model was selected in order to optimize energy production and consumption by adjusting the output power in the DFIG. The safe and effective use of the supercapacitor has been observed under optimal operating conditions [8-9]. In addition to ensuring optimum operating conditions, coordinated control was carried out in the DFIG using the supercapacitor in two stages for optimal active power control management [10]. The supercapacitor was selected in order to provide pitch angle control in the DFIG because of its advantages which include its high performance, high temperature operating ability, long service life, and convenient use in applications [11]. The effects of the supercapacitor in various DFIG short-circuit situations are discussed in detail. A hybrid model design was realized using the power electronics drives of a supercapacitor and a double-layer capacitor, and the response times in the transient state were improved [12-13]. The effects of the supercapacitor on small-signal stability were analyzed based on frequency stability, and the effects of the supercapacitor on the frequency ratio, operating mode, and participation factor were interpreted [14]. Transient analysis of the supercapacitor for active and reactive power control in a DFIG was examined. Moreover, short-circuit effects were minimized by providing flux and voltage control in the back-to-back converter circuit [15]. Depending on the maximum and minimum frequency values, the inertial model and the supercapacitor were used together in a DFIG for system reliability, and comparisons of conditions with and without supercapacitors were interpreted [16-19]. A supercapacitor was used for the static approach analysis of the energy storage system in a DFIG. In the static approach analysis, the energy storage level, energy storage cost, and wind speed distributions were discussed. With this approach, the average annual energy storage level, energy storage cost, hybrid energy storage, and wind speed distributions were determined, and situation analysis approaches were examined [20-22]. Another usage of the supercapacitor in DFIGs is to provide low voltage ride-through (LVRT) capability. Recovery from various symmetrical and asymmetrical faults with traditionally used DFIG control models may be insufficient. Various supercapacitor control models have been developed in DFIG for LVRT capability [23-24]. In this way, the adverse situations that may occur in grid-connected DFIGs can be eliminated. However, these models, which have been developed in some robust DFIG applications, may be insufficient due to inrush currents and over-voltages.

The aim of this study was to develop a different supercapacitor model in order to improve the stability, compensation, and oscillation damping of grid-connected DFIGs, especially in large power systems, while a dynamic model of the system was developed and studied in order to get a better transient-state time response. In this study, a two-layer, lookup table-based supercapacitor model was developed. An electrical model simulation was created as a two-layer supercapacitor mathematical model. The main contributions of this article are given below.

- Lookup table-based supercapacitor modeling in DFIG based wind turbines has developed.
- Mathematical correlation function for supercapacitor has created between the voltage and capacity.

- Sliding mode control has developed to coordinate the DC/DC converter and supercapacitor.
- Symmetrical and unsymmetrical faults with/without the enhanced supercapacitor has compared.

In section II.A of this study, the modeling of the DFIG is explained and in section II.B, the supercapacitor model is mentioned. In section II.C, the enhancement and control of the supercapacitor model in DFIG is explained mathematically in detail. In section II.D, the simulation study is presented and in section III, the results obtained from the simulation study are described, while the conclusion is detailed in the last section IV.

## II. MATERIAL AND METHODS

### A. MODELING OF THE DFIG

The circuit model of the DFIG, consisting of a gearbox, a rotor side converter (RSC), a grid side converter (GSC), and a crowbar unit, is shown in Figure 1.

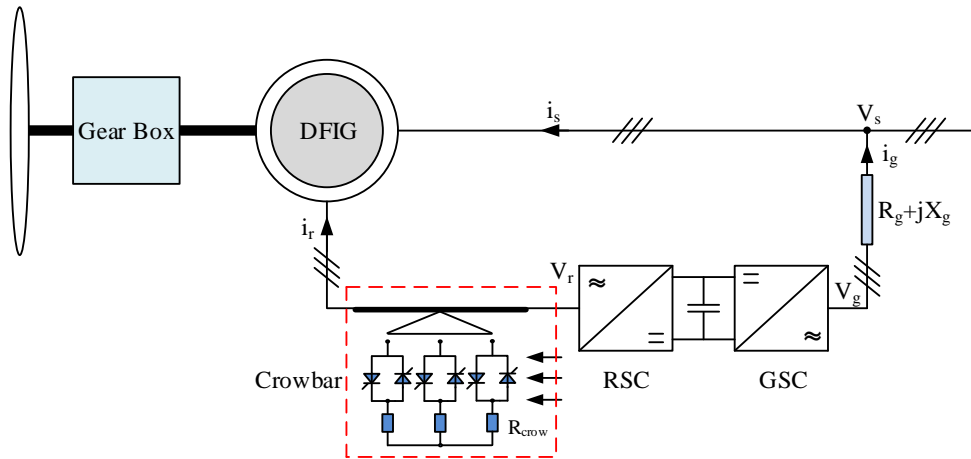


*Figure 1. Circuit model of the DFIG*

While the DFIG stator windings are directly linked to the grids, the rotor windings are linked to the grids via power electronics converters. These converters consist of two voltage source inverters with bidirectional current flow switching via pulse width modulation. The RSC circuit controls the electromagnetic torque, while the DC bus voltage is kept constant using the GSC circuit. With the three-phase windings in the stator and rotor circuit, the DFIG can take or give energy from both the stator and the rotor. Clarke and Park transforms are used in DFIG modeling [25-27] and d-q axis voltage and flux expressions have been developed for DFIG modeling. The d-q axis voltage expressions for the DFIG are shown in Equations (1) and (4).

$$V_{sd} = R_s i_{sd} - \omega_s \psi_{sq} + \frac{d\psi_{sd}}{dt} \quad (1)$$

$$V_{sq} = R_s i_{sq} + \omega_s \psi_{sd} + \frac{d\psi_{sq}}{dt} \quad (2)$$

$$V_{rd} = R_r i_{rd} - \omega_r \psi_{rq} + \frac{d\psi_{rd}}{dt} \quad (3)$$

$$V_{rq} = R_r i_{rq} + w_r \psi_{rd} + \frac{d\psi_{rq}}{dt} \quad (4)$$

The d-q axis flux relations in DFIG modeling are shown in Equations (5) and (8).

$$\psi_{sd} = L_s i_{sd} + L_m i_{rd} \quad (5)$$

$$\psi_{sq} = L_s i_{sq} + L_m i_{rq} \quad (6)$$

$$\psi_{rd} = L_r i_{rd} + L_m i_{sd} \quad (7)$$

$$\psi_{rq} = L_r i_{rq} + L_m i_{sq} \quad (8)$$

In the creation of the model, the expressions in Equations (5) and (8) are shortened to  $(L_s = L_{s\sigma} + L_m)$ ,  $(L_r = L_{r\sigma} + L_m)$ ,  $(\psi_{sd} = L_s i_{sd} + L_m i_{rd})$ ,  $(\psi_{sq} = L_s i_{sq} + L_m i_{rq})$ ,  $(\psi_{rd} = L_r i_{rd} + L_m i_{sd})$ , and  $(\psi_{rq} = L_r i_{rq} + L_m i_{sq})$ . The new versions of the d-q axis voltages are shown in Equations (9) – (12).

$$V_{sd} = R_s i_{sd} - w_s \psi_{sq} + L_{s\sigma} \frac{di_{sd}}{dt} + L_m \left( \frac{di_{rd}}{dt} + \frac{di_{sd}}{dt} \right) \quad (9)$$

$$V_{sq} = R_s i_{sq} + w_s \psi_{sd} + L_{s\sigma} \frac{di_{sq}}{dt} + L_m \left( \frac{di_{rq}}{dt} + \frac{di_{sq}}{dt} \right) \quad (10)$$

$$V_{rd} = R_r i_{rd} - w_r \psi_{rq} + L_{r\sigma} \frac{di_{sd}}{dt} + L_m \left( \frac{di_{rd}}{dt} + \frac{di_{sd}}{dt} \right) \quad (11)$$

$$V_{rq} = R_r i_{rq} + w_r \psi_{rd} + L_{r\sigma} \frac{di_{rq}}{dt} + L_m \left( \frac{di_{rq}}{dt} + \frac{di_{sq}}{dt} \right) \quad (12)$$

The new d-q axis voltage expressions obtained by using the flux-inductance relationship are shown in Equations (13) – (16).

$$V_{sd} = R_s i_{sd} - w_s ((L_{s\sigma} + L_m) I_{sq} + L_m + I_{rq}) + L_{s\sigma} \frac{di_{sd}}{dt} + L_m \left( \frac{di_{rd}}{dt} + \frac{di_{sd}}{dt} \right) \quad (13)$$

$$V_{sq} = R_s i_{sq} + w_s ((L_{s\sigma} + L_m) I_{sd} + L_m + I_{rd}) + L_{s\sigma} \frac{di_{sq}}{dt} + L_m \left( \frac{di_{rq}}{dt} + \frac{di_{sq}}{dt} \right) \quad (14)$$

$$V_{rd} = R_r i_{rd} - w_r ((L_{r\sigma} + L_m) I_{rq} + L_m + I_{sq}) + L_{r\sigma} \frac{di_{sd}}{dt} + L_m \left( \frac{di_{rd}}{dt} + \frac{di_{sd}}{dt} \right) \quad (15)$$

$$V_{rq} = R_r i_{rq} + w_r ((L_{r\sigma} + L_m) I_{rd} + L_m + I_{sd}) + L_{r\sigma} \frac{di_{rq}}{dt} + L_m \left( \frac{di_{rq}}{dt} + \frac{di_{sq}}{dt} \right) \quad (16)$$

where,  $\psi_{sd}$ ,  $\psi_{sq}$ ,  $\psi_{rd}$ , and  $\psi_{rq}$  are the stator-rotor phase winding fluxes,  $L_s$  and  $L_r$  are the stator-rotor phase winding inductances,  $L_m$  is the common inductance between stator and rotor,  $i_{sd}$ ,  $i_{sq}$ ,  $i_{rd}$ , and  $i_{rq}$

are the stator-rotor phase currents,  $w_s$  is the stator angular speed,  $V_{sd}$ ,  $V_{sq}$ ,  $V_{rd}$ , and  $V_{rq}$  are the  $d$ - $q$  axis stator-rotor voltages,  $R_s$  is the stator winding resistance,  $R_r$  is the rotor winding resistance, and  $I_{sd}$ ,  $I_{sq}$ ,  $I_{rd}$ , and  $I_{rq}$  are the  $d$ - $q$  axis stator-rotor current components, respectively.

Active and reactive power expressions produced by the DFIG modeling are shown in Equations (17) and (18).

$$P_s = V_{sd} I_{sd} + V_{sq} I_{sq} \quad (17)$$

$$Q_s = V_{sq} I_{sq} - V_{sd} I_{sd} \quad (18)$$

The relationship between the mechanical dynamic and the electrical torque obtained by using the angular speed ( $w_r$ ) of the rotor in the DFIG is shown in Equation (19).

$$T_{em} = N \frac{L_m}{L_s} (\psi_{sq} I_{rd} - \psi_{sd} I_{rq}) \quad (19)$$

where,  $N$  is the number of generator poles,  $T_m$  and  $T_{em}$  are the mechanical and electrical torques of the generator, respectively.

## B. SUPERCAPACITOR MODELING

Unlike conventional capacitors, supercapacitors consist of two solid electrodes with a liquid electrolyte. Solid electrodes make the supercapacitors double-layered [28-30]. An electron exchange is provided between the cathode and the anode. Accordingly, a capacity is formed between the electrode surfaces. Electrical circuit models are designed according to the operating conditions of the supercapacitors. The EPCOS supercapacitor model was used in the creation of this model [31]. The simple electrical equivalent model of the supercapacitor was formed by the Faranda model. The equivalent model of the supercapacitor is shown in Figure 2.

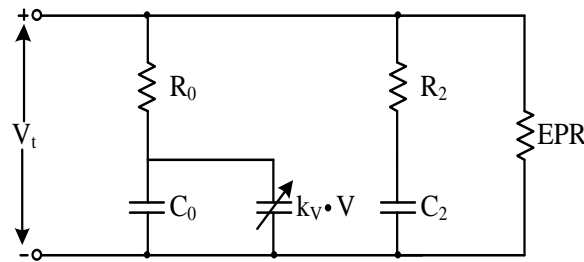


**Figure 2.** Faranda supercapacitor model

The model cell capacity expression is shown in Equation (20).

$$C_{cell} = C_0 + K_v V_c \quad (20)$$

The total capacity expressions for  $n$  numbers in the series for the model are shown in Equations (21) and (22).

$$C_{total} = \frac{1}{\frac{1}{C_{cell1}} + \frac{1}{C_{cell2}} + \frac{1}{C_{cell3}} \dots \dots \frac{1}{C_{celln}}} \quad (21)$$

$$C_{total} = \frac{1}{n} C_{cell} = \frac{1}{n} (K_v V_c) \quad (22)$$

The model terminal voltage equations and the capacity change over time are shown in Equations (23) – (25).

$$V(t) = i(t)R + \frac{1}{C_{total}} \int i(t)dt \quad (23)$$

$$V(t) = V_c(t) + (C_0 + K_v V_c)(R_0 + R_2) + \frac{dV_c(t)}{dt} \quad (24)$$

$$\frac{dV_c}{dt} = \frac{V - V_c}{(R_0 + R_2)(C_0 + K_v V_c)} \quad (25)$$

In the Faranda model, depending on the number of cells, the use of multiple resistors can be represented by equivalent series resistance (ESR) and equivalent parallel resistance (EPR). Voltage and initial voltage equations using equivalent series resistors are shown in Equations (26) – (28).

$$V(t) = R_{ESR}i(t) + \frac{1}{C_{total}} \int i(t)dt \quad (26)$$

$$V_0 = R_{ESR}i(t) + \frac{1}{C_{total}} \int i(t)dt \quad (27)$$

$$R_{ESR} + C_{total} \frac{di(t)}{dt} - i(t) = 0 \quad (28)$$

Charge and discharge expressions in the Faranda model are shown in Equations (29) and (30). The expression of the Faranda model terminal voltage ( $V_t$ ) as a function of time is shown in Equation (31).

$$V_r(t) = K e^{\frac{1}{R_{ESR} + C_{total}} t} \quad (29)$$

$$\frac{dV_c}{dt} = \frac{-V_c}{(R_0 + R_2)(C_0 + K_v V_c)} \quad (30)$$

$$V_t(t) = V_c(t) + V_r(t) \quad (31)$$

### C. ENHANCEMENT AND CONTROL OF THE SUPERCAPACITOR MODEL IN DFIG

Because the circuits created in the Faranda model are more conceptual than real functional circuits, their capacitor control and switching operations are not seen. Moreover, the Faranda model works effectively in steady-state studies and low power applications. However, studies on the transient situation are insufficient and contain too many errors. Therefore, it is more effective to use double-layer supercapacitor modeling instead of the Faranda model. The double-layer supercapacitor model is shown in Figure 3.

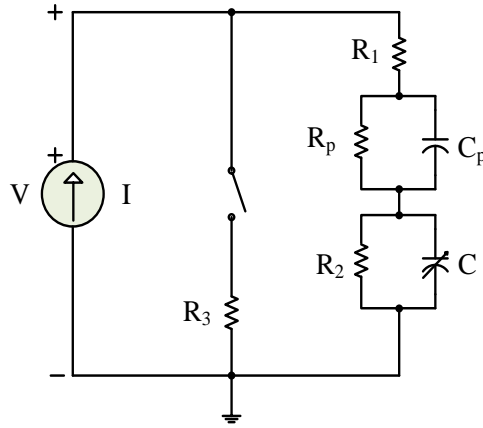


**Figure 3.** Double-layer supercapacitor model

In the double-layer supercapacitor circuit design, there are four resistors consisting of two capacitor groups. In adjusting the capacity according to the system dynamics, the lookup-table value is controlled depending on the voltage. This relationship is created using the voltage and voltage of derivation expression in Equations (32) and (33).

$$u_{LUP} = 7.1138 \times 10^{-8} t^3 + 1.1657 \times 10^{-3} t^2 + 6.4391 t - 11945 \quad (32)$$

$$\dot{u}_{LUP} = 2.13414 \times 10^{-7} t^2 + 2.3314 \times 10^{-3} t + 6.4391 \quad (33)$$

In double-layer supercapacitor modeling, the capacity-voltage relationship is designed based on a lookup table. The capacity value is obtained by implementing interpolation to the capacity-voltage curve in Figure 4.

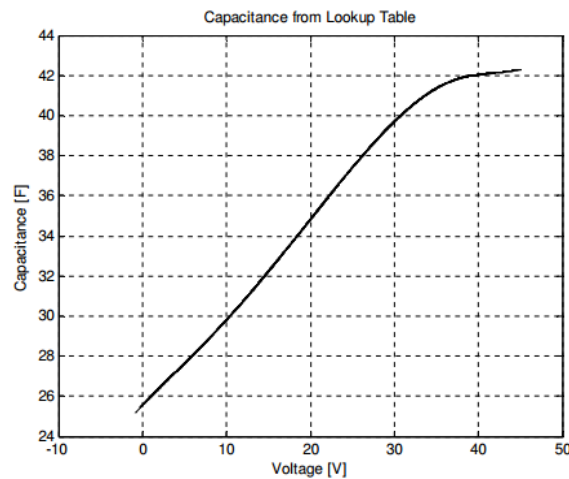


**Figure 4.** Capacity-voltage relationship of the supercapacitor

In the capacity-voltage curve of the supercapacitor it is seen that the capacity value increases as the voltage value increases. The process of selecting a capacity suitable for the 1200 V DC voltage in the simulation system was carried out according to this curve. The buck-boost converter circuit was designed so that the voltage value generated in the supercapacitor is equal to the DC voltage value. The output voltage ( $u_o$ ) and coil current ( $i_L$ ) for the dynamic state in the buck-boost converter circuit are shown in Equations (34) and (35).

$$\frac{du_0}{dt} = \frac{1}{C_0}[(1-D)i_L - \frac{u_0}{R_0}] \quad (34)$$

$$\frac{di_L}{dt} = \frac{1}{L}[u_D - (1-D)u_0] \quad (35)$$

The output voltage and coil current expressions for space state analysis are shown in Equation (36).

$$\begin{bmatrix} \dot{i}_L \\ \dot{u}_0 \end{bmatrix} = \begin{bmatrix} 0 & -(1-D)\frac{1}{L} \\ (1-D)\frac{1}{C_0} & \frac{1}{-RC_0} \end{bmatrix} \begin{bmatrix} i_L \\ u_0 \end{bmatrix} + \begin{bmatrix} \frac{1}{L} \\ 0 \end{bmatrix} u_D \quad (36)$$

A resistor, a coil and a capacitor are used in the buck-boost converter circuit. In this study, the buck-boost converter parameters chosen were: R (resistance) as 160, L (inductance) as 1 mH, and C (capacitor value) as 0.5 μF. Voltage adjustment based on the lookup table in the supercapacitor should be very sensitive. Otherwise, there may be problems in providing dynamic performance. However, with this sensitivity, the buck-boost converter should operate very smoothly [32-33]. Sliding mode control was used to ensure a harmonious coordination between the buck-boost converter and the supercapacitor. The state expression in systems with single input and output in sliding mode control is shown in Equation (37).

$$\dot{x} = f(x) + b(x)u \quad (37)$$

where,  $x$  is the state variable,  $u$  is the input variable, and  $f(x)$  and  $b(x)$  are defined as the limited nonlinear functions of state variables. The basic principle of sliding mode control is to use switching control logic to force the trajectories of the dynamic variable structure system to follow a particular path called the “sliding surface”. Trajectories use the time-varying floating surface expression for the system to determine the error, as shown in Equation (38).

$$S(x;t) = \left(\frac{d}{dt} + \lambda\right)^{n-1} x \quad (38)$$

where  $x$  is the trajectory error in state  $x$ ,  $\lambda$  is the positive constant coefficient, and  $n$  is the order of the system in operating state. The expression that allows the system to operate in the desired orbit is shown in Equation (39).

$$\frac{1}{2} \frac{d}{dt} S^2 \leq -\mu(S) \quad (39)$$

where  $\mu$  is the constant positive value. In sliding mode control, in the buck-boost converter switching technique, the sliding surface continuously creates a high frequency around the sliding surface (S), with a chattering effect. Therefore, sliding mode control is generally applied to nonlinear systems. For this purpose, the linearization process is performed in the supercapacitor model, which makes it very simple to apply the sliding mode control on the energy storage system elements. The voltage-capacity relationship is used in the linearization process. The sliding mode surface consists of the expression of S as the current error. The amount of current error in the current loop for sliding mode control is shown in Equation (40).

$$S = i_L^* - i_L \quad (40)$$

where  $S = 0$  is the desired state. The sliding mode control study has two main functions: the control function and modulator function. Therefore, the sliding mode output control is the duty cycle ( $D$ ). The sliding model-based duty cycle statement is shown in Equation (41).

$$D = \frac{1}{2}(1 - \text{sign}(S)) \quad (41)$$

To follow the current reference in the sliding mode control, the output DC voltage must be higher than the limit given in Equation (42) below.

$$U_0 \geq \frac{3}{2} \sqrt{(V_g^{\max})^2 + (L_{inv} \times 2\pi f \times I_g^{\max})^2} \quad (42)$$

where,  $V_g^{\max}$  is the maximum grid voltage,  $L_{inv}$  is the phase inductance,  $I_g^{\max}$  is the maximum grid current, and  $f$  is the frequency, respectively. With the sliding mode control, the buck-boost converter output voltage increases to the desired voltage level. Moreover, with the sliding mode control, the dynamic behavior of the  $R_p$  and  $C_p$  elements used in the supercapacitor can be controlled very quickly. With the supercapacitor added to the DC bus, the GSC circuit works as an active power source. The connection of the supercapacitor in the DFIG is shown in Figure 5.

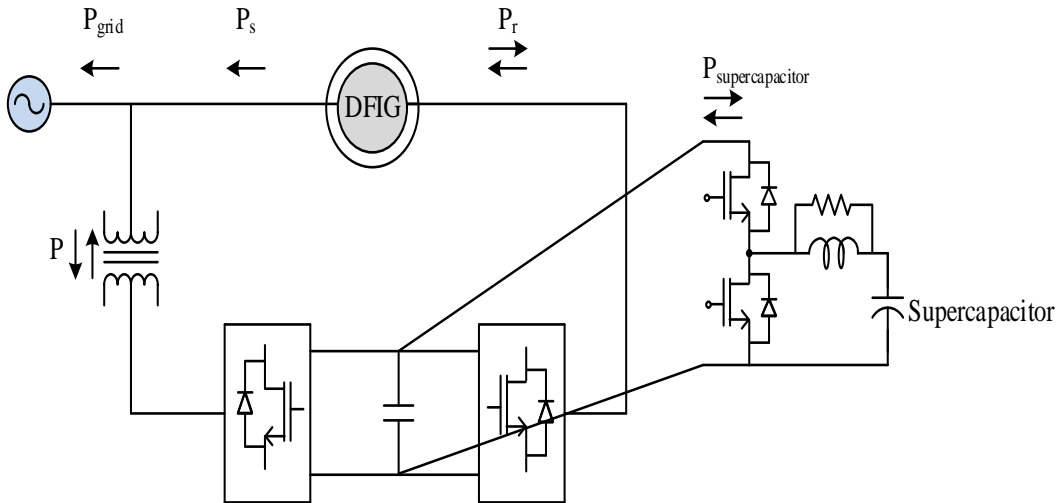


**Figure 5.** The connection of the supercapacitor in the DFIG

In the DFIG, the supercapacitor is able to adjust the DC bus voltage value in the range of 0-100%. While a certain part of the power values are met by the grid in the creation of the supercapacitor model, the remaining power values are met by the DFIG. The amounts of energy and capacity expressions stored in the supercapacitor are shown in Equations (43) – (45).

$$E_{supercapacitor} = 0.2P_{nominal}t \quad (43)$$

$$E_{supercapacitor} = \frac{1}{2}C_{supercapacitor}(V_{max}^2 - V_{min}^2) \quad (44)$$

$$C_{supercapacitor} = \frac{0.4P_{nominal}t}{(V_{max}^2 - V_{min}^2)} \quad (45)$$

where,  $E_{supercapacitor}$  is the amount of energy in the supercapacitor,  $P_{nominal}$  is the nominal power value,  $t$  is the supercapacitor operating time,  $C_{supercapacitor}$  is the supercapacitor capacity value,  $V_{max}$  is the

maximum supercapacitor voltage, and  $V_{min}$  is the minimum supercapacitor voltage, respectively. The supercapacitor model developed based on a double-layer lookup table with sliding mode control is shown in Figure 6.

The developed supercapacitor model is activated during a transient situation in the DFIG. Under steady-state operation, the system control provides DC link voltage. Under steady-state operation the DC/DC converter circuit used in the DFIG can adjust the DC voltage depending on the amount desired. A time-related switching element is used for the activation of the supercapacitor. The difference between the measured and reference values enters the controller. The switching element of the converter on the grid side is triggered by making the desired level adjustment on the controller.  $R_1$  resistance determines losses during charge and discharge in developed supercapacitor model.  $R_2$  resistance controls the charge and discharge effect in the developed supercapacitor model.  $R_3$  resistance protects the supercapacitor against overvoltages during transient state. The  $R_p$  resistance and the  $C_p$  capacitor observe the dynamic behavior of the supercapacitor during the transient state. In this study, the supercapacitor was not used in the continuous operation of the system. The supercapacitor worked in the power system-connected DFIG according to symmetrical and asymmetrical short-circuit events occurring on the grid side.

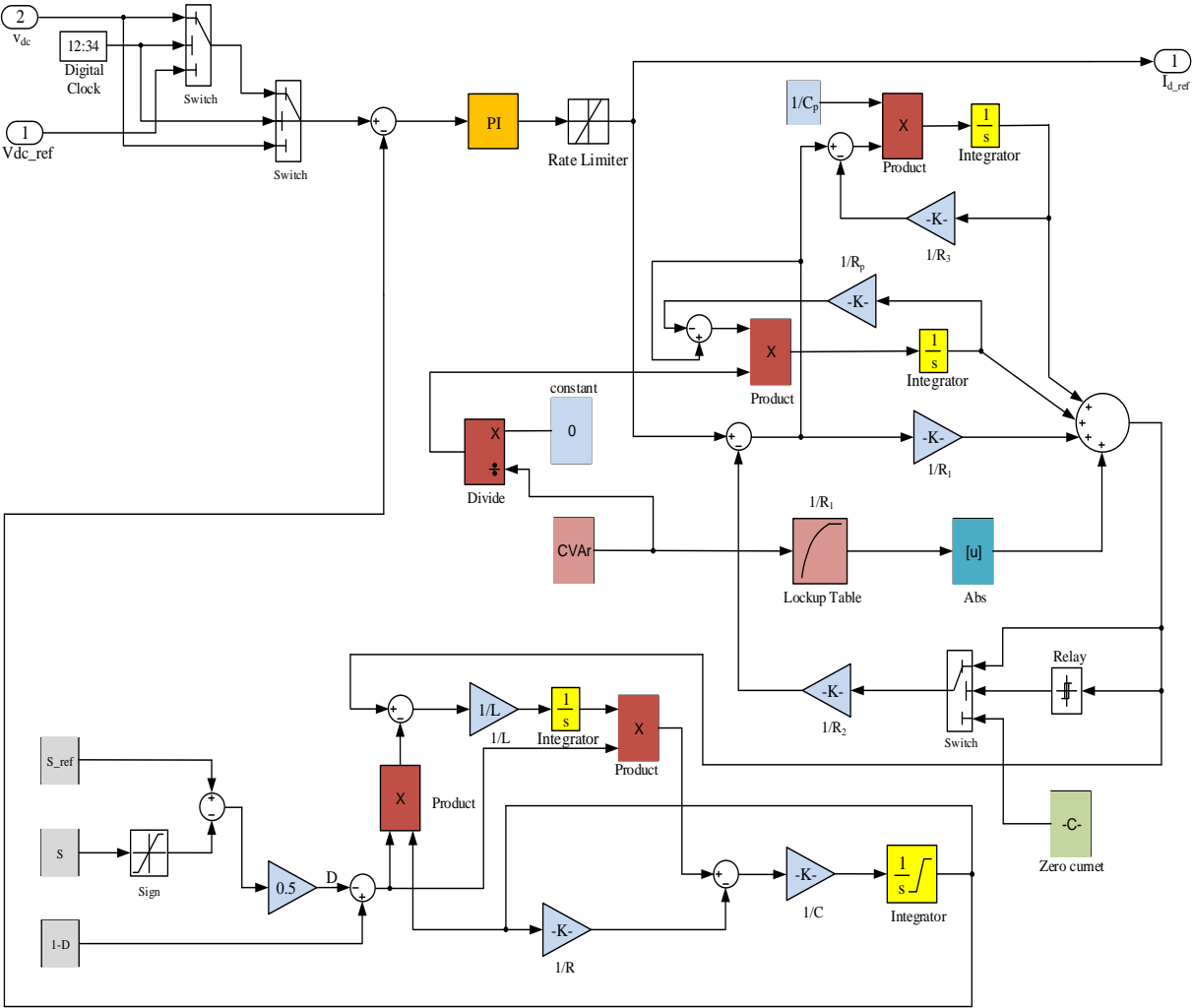


Figure 6. Developed supercapacitor model

## D. SIMULATION MODEL

The model simulated in this study is shown in Figure 7.

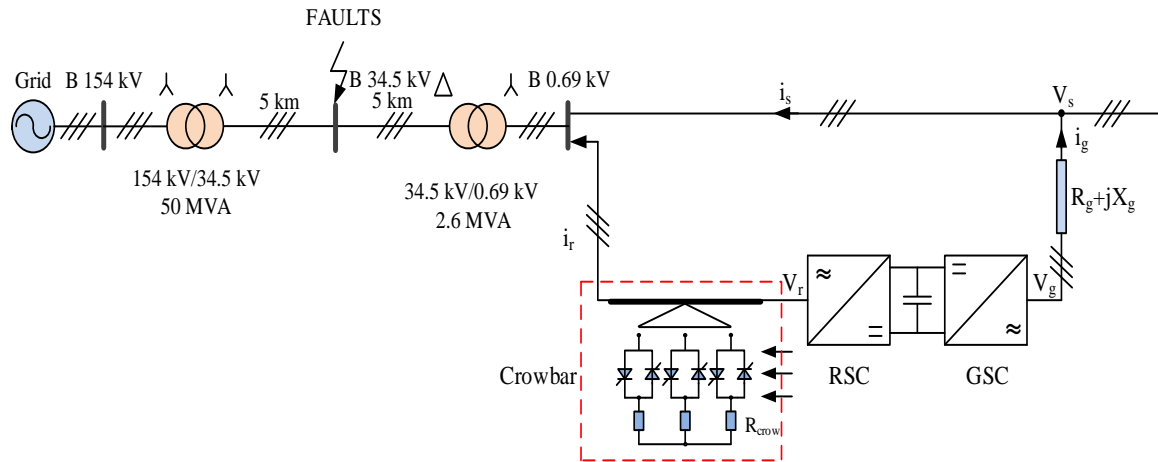


Figure 7. Test system

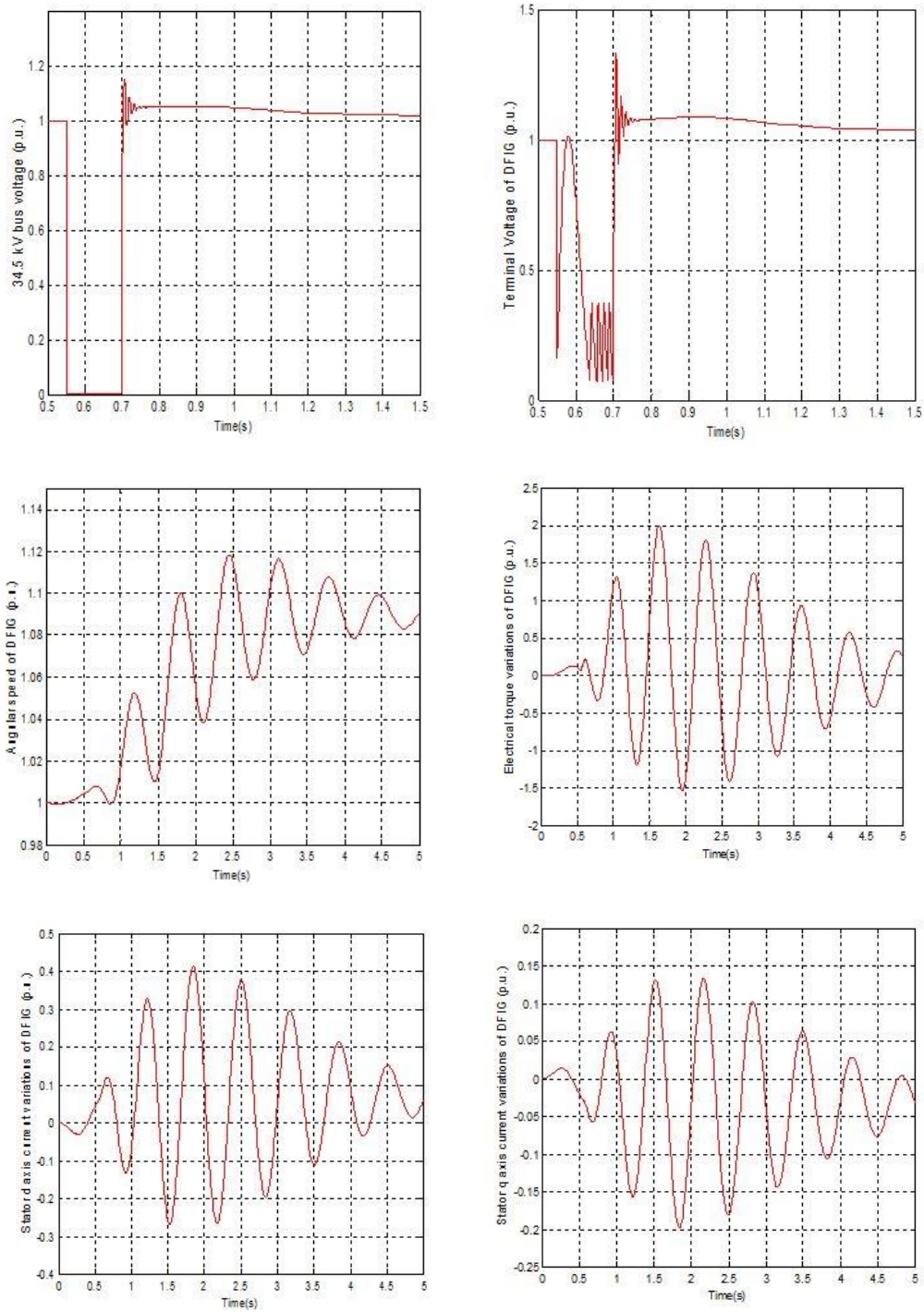
The simulation model used a 154-kV grid. In this system, a transformer was used to reduce 154 kV to 34.5 kV. Moreover, a 10-km long medium-length pi transmission line was used. At the output of the transmission line, a transformer was used to reduce 34.5 kV to 690 V. There were 2.3 MW DFIG-based wind turbines at the output of 690 V transformers. The transformer power on the grid side was selected as 50 MVA, while the power value of 2.6 MVA was selected at the DFIG output. Saturation rates of both transformers were ignored. The DFIG parameter values, transformers, and grid voltage in the DFIG output were established as design values and the operating status of the wind turbine made in Turkey was determined. Symmetrical and asymmetrical faults occurred in the 154 kV bus. A 3-phase fault was selected as the symmetrical fault, while a ground fault was selected as the asymmetrical fault. Analyses of the presence and absence of the supercapacitor in the DFIG-based wind turbine were examined. The parameters used in the DFIG are given in Table 1.

Table 1. DFIG parameters

Parameters	stator resistance	rotor resistance	stator inductance	rotor inductance	magnetization inductance	inertia constant
Value	0.00706 $\Omega$	0.005 $\Omega$	0.171 H	0.156 H	2.9 H	3.5

## III. SIMULATION MODEL RESULTS

The first analysis in this study was of the 3-phase fault that occurred between 0.55 s and 0.7 s. In the case of the 3-phase fault, a comparison was made of the conditions where the supercapacitor was used and not used. The bus voltage variations and changes in DFIG parameters are shown in Figures 8 and 9.



**Figure 8.** 3-phase fault results obtained without the supercapacitor

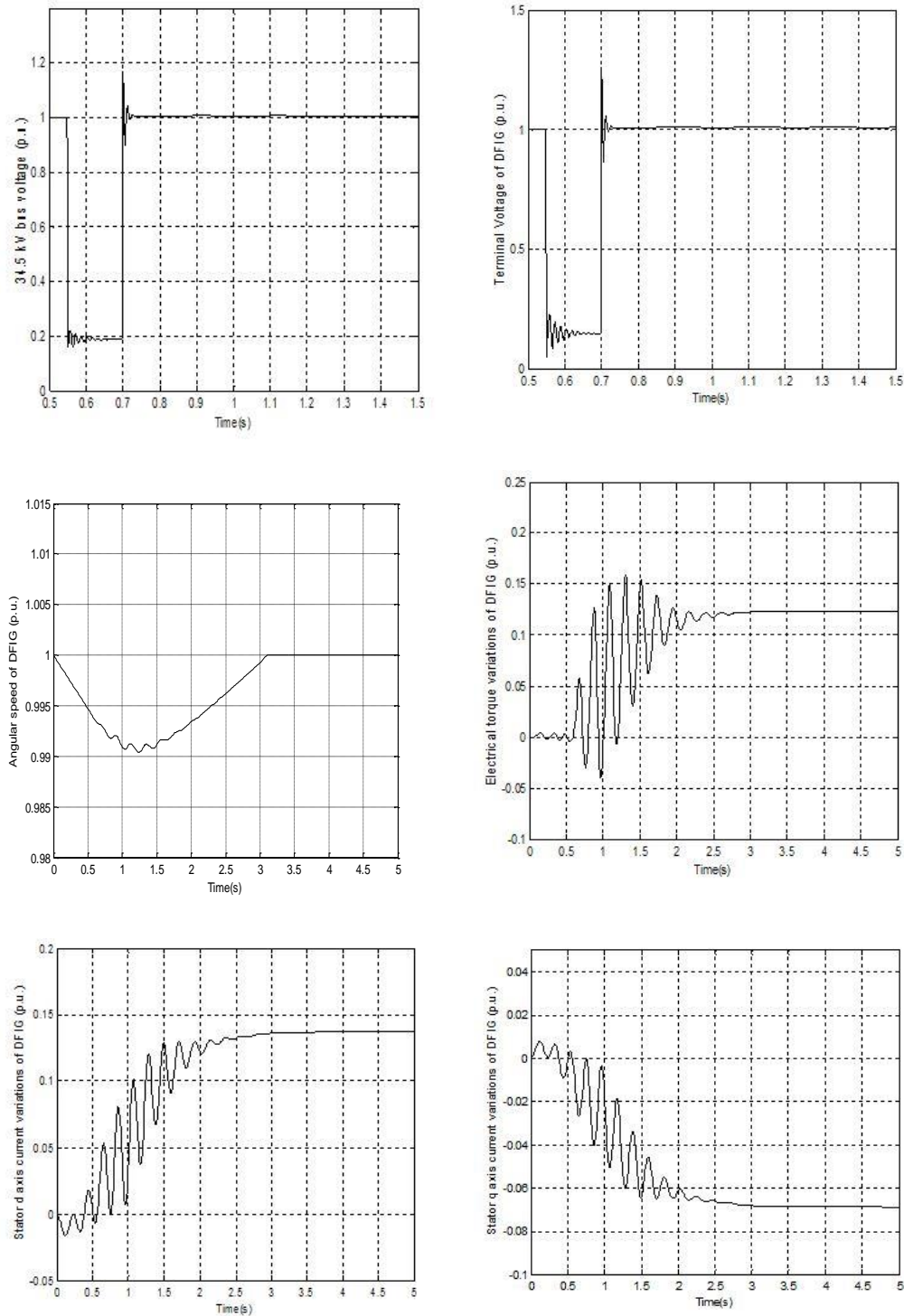


**Figure 9.** 3-phase fault results obtained with the supercapacitor

As a result of the 3-phase fault analysis, when the supercapacitor was used, the 34.5 kV bus voltage of 0.0 p.u. rose to the value of 0.195 p.u. Similarly, the output voltage of the DFIG of 0.15 p.u. rose to the value 0.2 p.u. When the oscillation ranges of all parameter values were examined, it was observed that the values had increased. Without the use of the supercapacitor, the 34.5 kV bus voltage was 0.0–1.15 p.u., DFIG output voltage 0.1–1.32 p.u., angular velocity 1–1.12 p.u., electrical moment -1.5–2 p.u., and d-q axis stator current changes -0.28–0.41 p.u. and -0.2–0.125 p.u., respectively. When the supercapacitor was used, oscillation ranges for the 34.5 kV bus voltage were 0.195–1.7 p.u., DFIG output voltage 0.15–1.25 p.u., angular velocity 0.992–1.0 p.u., electrical moment -0.04–0.155 p.u., and d-q axis stator current changes -0.01–0.135 p.u. and -0.065–0.01 p.u., respectively. In the simulation

study, a ground fault was examined as the second analysis. In the ground fault of between 0.55 s and 0.7 s, the bus voltages and the changes in the DFIG parameters were examined according to whether or not the supercapacitor was used. The results obtained are shown in Figures 10 and 11.

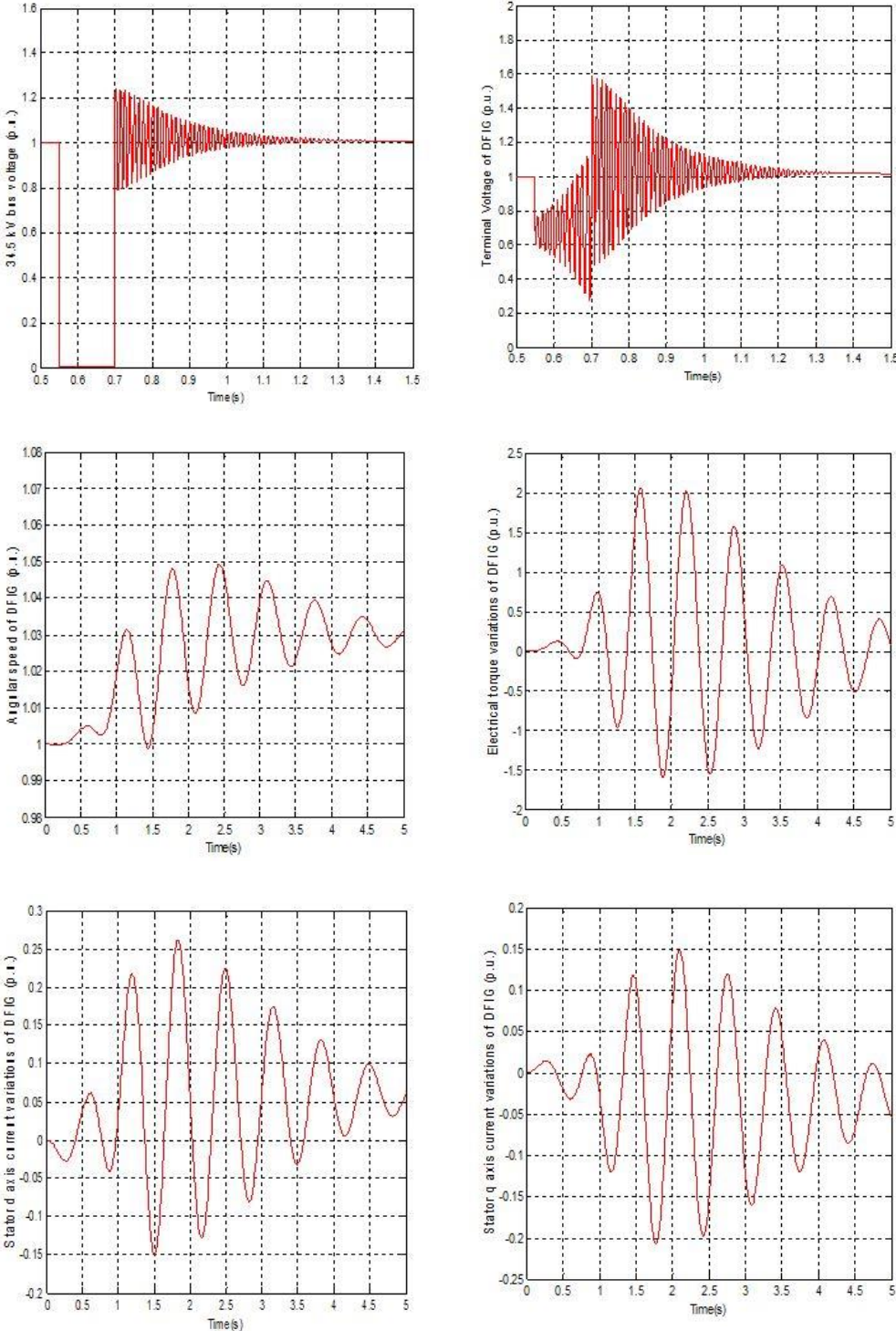
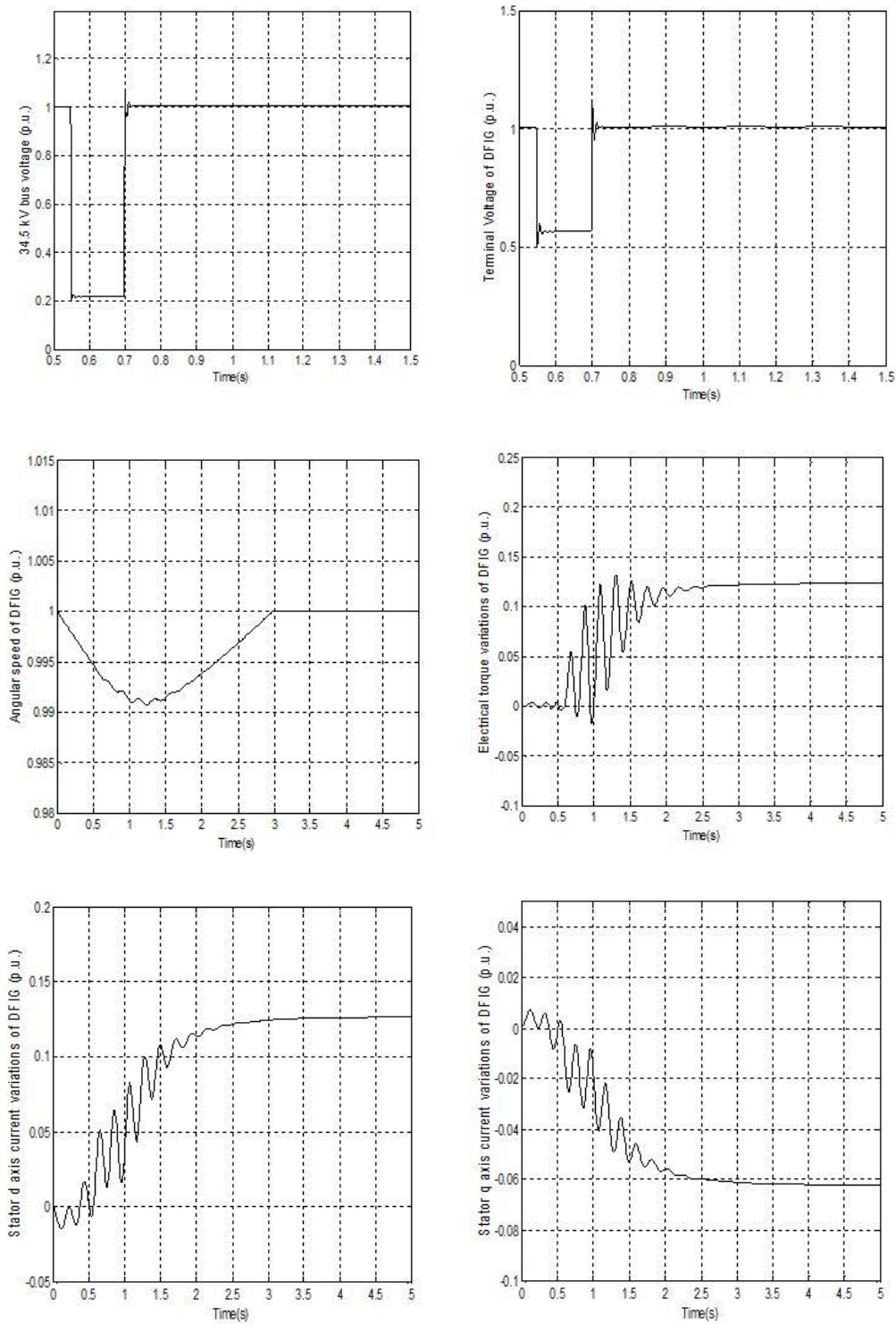


Figure 10. A phase ground fault results without the supercapacitor



**Figure 11.** A phase ground fault results with the supercapacitor

In the case of the ground fault that occurred between 0.55 s and 0.75 s, the 34.5 kV bus voltage was increased from 0.0 p.u. to the value of 0.2 p.u. The output voltage of the DFIG increased from 0.3 p.u. to 0.58 p.u. When the oscillation conditions of the parameters in the ground fault in the system were examined, without the supercapacitor, the 34.5 kV bus voltage was 0.0–1.22 p.u., DFIG output voltage 0.25–1.59 p.u., angular velocity 1–1.05 p.u., electrical torque -1.55–2.05 p.u., and d-q axis stator current changes -0.15–0.26 p.u. and -0.205–0.15 p.u., respectively. When the supercapacitor was used in the system, the oscillation ranges of the 34.5 kV bus voltage were 0.2–1.07 p.u., DFIG output

voltage 0.58–1.12 p.u., angular velocity 0.99–1.0 p.u., electrical moment 0.01–0.125 p.u., and d-q axis stator current changes -0.01–0.125 p.u. and -0.625–0.006 p.u., respectively.

## **V. CONCLUSIONS**

The use of energy storage elements plays an important role in theoretically resolving transient problems in grid-connected DFIG-based wind turbines. This study discussed in detail the effects of a supercapacitor, as an energy storage system element, on the DFIG in the case of transient stability. It was observed that the developed lookup table- and sliding mode-based supercapacitor model gave quite effective results for both symmetrical and asymmetrical faults. As a result of the fault analysis, bus voltages and DFIG parameters promptly became stabilized. It was observed that the 34.5 kV bus voltage and the DFIG output voltage were compensated during the faults. Moreover, it was observed that the oscillations occurring after the symmetrical and asymmetrical faults were quickly damped. In the DFIG, the parameter most affected by the symmetrical and asymmetrical faults was the electrical torque, while the q-axis stator current variations were the least affected.

**ACKNOWLEDGEMENTS:** The authors declare that they have no conflict of interest.

## **VI. REFERENCES**

- [1] W.C. de Carvalho, R.P. Bataglioli, R.A. Fernandes, and D.V. Coury, “Fuzzy-based approach for power smoothing of a full-converter wind turbine generator using a supercapacitor energy storage,” *Electric Power Systems Research*, vol. 184, no. 106287, 2020.
- [2] I.M. Syed, B.Venkatesh, B. Wu, and A.B. Nassif, “Two-layer control scheme for a supercapacitor energy storage system coupled to a doubly fed induction generator,” *Electric Power Systems Research*, vol.86, pp. 76-83, 2012.
- [3] Q. Liyan and W. Qiao, “Constant power control of DFIG wind turbines with supercapacitor energy storage,” *IEEE Transactions on Industry Applications*, vol. 47, pp. 359-367, 2011.
- [4] V. Krishnamurthy and C.R. Kumar, “A novel two layer constant power control of 15 DFIG wind turbines with supercapacitor energy storage,” *International Journal of Advanced and Innovative Research*, vol. 2, pp. 68-77, 2013.
- [5] S. Dongyang, Z. Xiongxin, S. Lizhi, W. Fengjian, and Z. Guangxin, “Study on power fluctuation suppression of DFIG based on super capacitor energy storage,” in *2017 IEEE Conference on Energy Internet and Energy System Integration (EI2)*, IEEE, 2017, pp. 1-6.
- [6] R. Suryana, “Frequency control of standalone wind turbine with supercapacitor,” in *2011 IEEE 33rd International Telecommunications Energy Conference (INTELEC)*, IEEE, 2011, pp. 1-8.
- [7] R. Aghatehrani, R. Kavasseri, and R.C. Thapa, “Power smoothing of the DFIG wind turbine using a small energy storage device,” in *IEEE PES General Meeting*, IEEE, 2010, pp. 1-6.
- [8] N. Mendis, K.M. Muttaqi, and S. Perera “Active power management of a supercapacitor-battery hybrid energy storage system for standalone operation of DFIG based wind turbines,” in *IEEE Industry Applications Society Annual Meeting*, Las Vegas, USA, 2012, pp. 1-8.

- [9] E. Naswali, C. Alexander, H.Y. Han, D. Naviaux, A. Bistrika, A.V. Jouanne, A. Yokochi, and K.A.T. Brekken, "Supercapacitor energy storage for wind energy integration," in *IEEE Energy Conversion Congress and Exposition*, Phoenix, Arizona, 2011, pp. 298-305.
- [10] S. Huang, Q. Wu, Y. Guo, and F. Rong, "Optimal active power control based on MPC for DFIG-based wind farm equipped with distributed energy storage systems," *International Journal of Electrical Power & Energy Systems*, vol. 113, pp. 154-163, 2019.
- [11] T. Wei, S. Wang, and Z. Qi, "Design of supercapacitor based ride through system for wind turbine pitch systems," in *2007 International Conference on Electrical Machines and Systems (ICEMS)*, IEEE, 2007, pp. 294-297.
- [12] S.M. Muyeen, R. Takahashi, M.H. Ali, T. Murata, and J. Tamura, "Transient stability augmentation of power system including wind farms by using ECS," *IEEE Transactions on Power Systems*, vol. 23, no. 3, pp. 1179-1187, 2008.
- [13] N. Mendis, K.M. Muttaqi, S. Sayeef, and S. Perera, "Application of a hybrid energy storage in a remote area power supply system," in *2010 IEEE International Energy Conference*, IEEE, 2010, pp. 576-581.
- [14] X. Li, C. Hu, C. Liu, and D. Xu, "Modeling and control of aggregated super-capacitor energy storage system for wind power generation," in *2008 34th Annual Conference of IEEE Industrial Electronics*, IEEE, 2008, pp. 3370-3375.
- [15] H. Babazadeh, W. Gao, and X. Wang, "Controller design for a hybrid energy storage system enabling longer battery life in wind turbine generators," in *2011 North American Power Symposium*, IEEE, 2011, pp. 1-7.
- [16] M.F.M Arani, and E.F. El-Saadany, "Implementing virtual inertia in DFIG-based wind power generation," *IEEE Transactions on Power Systems*, vol. 28, pp. 1373-1384, 2013.
- [17] D. Yang, H.C. Gao, L. Zhang, T. Zheng, L. Hua, and X. Zhang, "Short-term frequency support of a doubly-fed induction generator based on an adaptive power reference function," *International Journal of Electrical Power & Energy Systems*, vol. 119, 2020.
- [18] J. Zhu, J. Hu, W. Hung, C. Wang, X. Zhang, S. Bu, and C.D. Booth, "Synthetic inertia control strategy for doubly fed induction generator wind turbine generators using lithium-ion supercapacitors," *IEEE Transactions on Energy Conversion*, vol. 33, no. 2, pp. 773-783, 2017.
- [19] L. Xiong, Y. Li, Y. Zhu, P. Yang and Z. Xu, "Coordinated control schemes of super-capacitor and kinetic energy of DFIG for system frequency support," *Energies*, vol. 11, no. 1, 2018, doi: 10.3390/en11010103.
- [20] A.M. Gee, F.V. Robinson, and R.W. Dunn, "Analysis of battery lifetime extension in a small-scale wind-energy system using supercapacitors," *IEEE Transactions on Energy Conversion*, vol. 28, no. 1, pp. 24-33, 2013.
- [21] K.W. Wee, S. S. Choi, and D.M. Vilathgamuwa, "Design of a least-cost battery-supercapacitor energy storage system for realizing dispatchable wind power," *IEEE Transactions on Sustainable Energy*, vol. 4, no. 3, pp. 786-796, 2013.
- [22] H. Babazadeh, W. Gao, J. Lin, and L. Cheng, "Sizing of battery and supercapacitor in a hybrid energy storage system for wind turbines," in *PES T&D 2012*, IEEE, 2012, pp. 1-7,

- [23] S.S. Sahoo, K. Chatterjee, and P.M. Tripathi, "A coordinated control strategy using supercapacitor energy storage and series dynamic resistor for enhancement of fault ride-through of doubly fed induction generator," *International Journal of Green Energy*, vol. 16, no. 8, pp. 615-626, 2019.
- [24] O. Noureldeen and M.M. Youssef, "Super-capacitor utilization for low-voltage ride through improvement of grid-tied wind turbines," in *2017 Nineteenth International Middle East Power Systems Conference (MEPCON)*, IEEE, 2017, pp. 1305-1309.
- [25] A. Luna, F.D.A Lima, D. Santos, P. Rodríguez, E.H. Watanabe, and S. Arnaltes, "Simplified modeling of a DFIG for transient studies in wind power applications," *IEEE Transactions on Industrial Electronics*, vol. 58, no. 1, pp. 9-20.
- [26] L. Yang, Z. Xu, J. Ostergaard, Z.Y. Dong, and K.P. Wong, "Advanced control strategy of DFIG wind turbines for power system fault ride through," *IEEE Transactions on Power Systems*, vol. 27, no. 2, pp. 713-722, 2011.
- [27] P.C. Krause, O. Wasynczuk, S.D. Sudhoff, and S. Pekarek, *Analysis of Electric Machinery and Drive Systems*, 3rd ed., vol. 75, New Jersey, USA: John Wiley & Sons, 2013, pp. 75-100.
- [28] A.B. Cultura and Z.M. Salameh, "Modeling, evaluation and simulation of a supercapacitor module for energy storage application," in *International Conference on Computer Information Systems and Industrial Applications*, 2015, pp. 876-882.
- [29] M.K. Döşoğlu and A.B Arsoy, "Transient modeling and analysis of a DFIG based wind farm with supercapacitor energy storage," *International Journal of Electrical Power & Energy Systems*, vol. 78, pp. 414-421, 2016.
- [30] M. K. Döşoğlu, "Nonlinear dynamic modeling for fault ride-through capability of DFIG-based wind farm," *Nonlinear Dynamics*, vol. 89, no. 4, pp. 2683-2694, 2017.
- [31] *Data Sheet for Supercapacitor from EPCOS*, Part No.: B48621–S0203-Q288, 2011.
- [32] M. Firouzi, M. Nasiri, S. Mobayen, and G.B. Gharehpetian, "Sliding mode controller-based BFCL for fault ride-through performance enhancement of DFIG-based wind turbines," *Complexity*, vol. 2020, no. 1259539, pp. 1-12, 2020.
- [33] M. Gaiceanu, "MATLAB/simulink-based grid power inverter for renewable energy sources integration," *MATLAB-a Fundamental Tool for Scientific Computing and Engineering Applications*, vol. 3 pp. 1-219, 2012.